Transdermal Electrophysiological Recordings of Diabetic Peripheral Neuropathy Using a Needle Electrode Array in Mice and Men

Magdalena Blaszkiewicz[1,3], Lydia Caron[3], Brooke Villinski[2], Joshua Passarelli[3], Jonathan Donnelly[4], Julia M. Towne[2], Naeemah M. Story[1], Erin Merchant[2], Furrukh S. Khan[5], Nuri Emanetoglu[2], Leonard Kass[3], Rosemary L. Smith[2]*, Kristy L. Townsend[1,3]*

Author affiliations:

[1]Department of Neurological Surgery, The Ohio State University, Columbus, OH

[2] College of Engineering, University of Maine, Orono, ME

[3] School of Biology and Ecology, University of Maine, Orono, ME

[4] Computer Science, University of Maine, Orono, ME

[5] Department of Electrical & Computer Engineering, The Ohio State University, Columbus, OH

*Co-Corresponding Authors:

kristy.townsend@osumc.edu

460 W 12th Ave, 1014 Biomedical Research Tower, Columbus OH

ORCID: 0000-0002-2849-9195

rosemary.smith@maine.edu

Department of Electrical and Computer Engineering, The University of Maine, Orono, ME 04469

ABSTRACT

Diabetic peripheral neuropathy (DPN) is one of the most common complications of diabetes. Proactive treatment options remain limited, largely due to a lack of sensitive and convenient diagnostics, especially early in disease progression or specifically for small fiber neuropathy (SFN), the dying back of distal small diameter nerves. Here, we report on the design, testing, and validation of a novel medical diagnostic device for the functional assessment of small fiber nerves: an electrically conductive needle array designed to record nerve activity signals in the skin and transdermal tissues, which we call the DEN (Detecting Early Neuropathy). DEN recordings were validated across a time course of high fat diet-induced DPN in mice. Based on preclinical mouse data, the device was then adapted to obtain recordings in human tissue. DEN recordings successfully recorded various types of neural activity. New functional diagnostic tools like DEN offer a promising outlook for patients needing an earlier and more sensitive diagnosis of SFN/DPN, which will allow for earlier and more effective treatment options such as implementation of glucose regulation strategies.

Keywords: adipose tissue, diabetes, obesity, medical device, needle electrodes, microneedle, peripheral nerves, diabetic peripheral neuropathy, small fiber nerve recording, transdermal electrophysiology

Abbreviations

CAN	Cardiovascular autonomic neuropathy
CAP	Compound action potential
CMAP	Compound muscle action potential
DEN	Detecting early neuropathy
DPN	Diabetic peripheral neuropathy
EKG	Electrocardiogram
EMG	Electromyography
HFND	High fat neuropathy diet
HPF	High pass filter

IENF	Intra-epidermal Nerve Fibers
LPF	Low pass filter
PBC	Printed circuit board
PN	Peripheral neuropathy
PAP	Putative action potential
SFN	Small fiber neuropathy
scWAT	Subcutaneous white adipose tissue
SiLN	Subiliac lymph node
WAT	White adipose tissue

INTRODUCTION

An estimated 30 million Americans suffer from a progressive and debilitating disease known as peripheral neuropathy (PN). More than 30 medical conditions can lead to this disease, which is marked by a progressive dying back of distal nerves that typically starts in the skin of the extremities (arms and legs), and moves inward to deeper tissue layers. Most cases of PN are a polyneuropathy with several nerve subtypes affected (sensory, autonomic, motor), which subsequently leads to complex symptoms ranging from pain, tingling and burning, to loss of sensation, numbness, and in severe cases can even lead to limb amputation[1]. These drastic clinical outcomes are often due to a lack of effective diagnostic tools to provide an early and sensitive diagnosis of neuropathy, which would impact the clinical course of care. Currently, there is no cure for peripheral neuropathy to halt nerve degradation and re-innervate tissues, and treatments primarily focus on management of symptoms and palliative care. However, for certain peripheral neuropathies, a timely diagnosis can enable interventions to prevent further decline[2], such as for diabetic peripheral neuropathy (DPN) where better glucose control can be achieved to mitigate the PN. The availability of a better functional measurement of PN, particularly for small fiber PN versus large fiber PN, for which there already are several clinical measurement options for detecting large fiber nerve activity, would also improve monitoring as new treatments are developed and made available to patients. Since peripheral nerves can uniquely re-grow compared to nerves in the brain, better functional diagnostics may provide earlier windows of interventions and opportunities for new treatments that target tissue re-innervation.

Diabetic Peripheral Neuropathy (DPN) and Small Fiber Neuropathy (SFN)

Diabetes mellitus is a chronic disease characterized by insulin insufficiency (type 1) or insulin resistance (type 2), which in turn affects whole body energy homeostasis. Diabetes has the highest incidence rate of any metabolic disease in the world[3], and is associated with numerous co-morbidities and increased mortality. The International Diabetes Federation estimates that over 463 million individuals have diabetes. It is estimated that 50% or more[4] of type 2 diabetics develop peripheral neuropathy at some stage of the disease, while the range for prediabetics is wider, at an estimated 2%-77%. The majority of studies show a PN prevalence greater or equal to 10%,[5] making it the most prevalent complication of diabetes[6]. Additionally, diabetes is now the leading cause of PN, closely followed by aging/idiopathic. Since diabetes risk increases with age, many diabetic cases are also age-related PN. More recently, COVID-19 has become a new cause of PN[7]. Over time it is thought that chronic hyperglycemia with diabetes causes damage to the

capillaries and peripheral nerves of the extremities[8]. Other leading hypotheses implicate lipotoxicity instead of glucotoxicity, or a degenerative outcome from chronic inflammation[9]. Unlike nerves of the central nervous system, peripheral nerves can regenerate (to a certain extent) following nerve injury, and regardless of the initial trigger, in PN once initial damage to the nerves begins taking place, the initial response of the PNS is a regenerative one. During peripheral nerve regeneration a phenomenon known as sprouting occurs, where the injured axons of peripheral nerves begin forming many new branches[10]. In DPN, where the insult to nerves is continuous, this sprouting process can be prolonged and affect uninjured nerves thereby contributing to increased pain sensation[10]. This often causes individuals suffering from early stages of peripheral neuropathy to go through a period of hypersensitivity of the peripheral nerves, which can be painful. Following this hypersensitive period, progressive neural damage ultimately causes nerves to die back proximally, in a length dependent manner (longer axons in distal extremities first) and from the skin surface down to deeper tissue layers, including, as we have demonstrated[11-13] in subcutaneous white adipose tissue (scWAT). Small fiber nerve death can also progress to large fiber neuropathy, making this overall a progressive and degenerative condition. Although peripheral nerves are capable of regeneration, something in PN and DPN blunts the ability of tissues to recover proper innervation. Particularly relevant in DPN, the neuropathy of metabolically important tissues such as muscle and adipose may further exacerbate the disease. Adipose tissue nerves are known to be essential for lipolysis, thermogenesis, and other tissue functions, and thus loss of this essential nerve supply can have detrimental effects on metabolic control.

Small fiber neuropathy (SFN) is the result of damage to both myelinated and unmyelinated small diameter peripheral nerves (0.2-1.5 μm in diameter) that innervate tissues and organs, as branches from larger nerve bundles. In SFN, small somatic and autonomic fibers can be affected, which control thermal and pain perception, as well as autonomic and enteric functions[14]. As a result, patients with SFN can present with either autonomic or somatic symptoms, or a combination. Symptoms of small fiber neuropathy can include allodynia, burning, decreased thermal sensation, hyperesthesia, paresthesia, numbness in the extremities, restless leg syndrome, dry eyes and mouth, abnormal sweating, bladder control issues, gastric issues, skin discoloration, and cardiac symptoms such as syncope, palpitations, and orthostatic hypotension. As a disease, the pathology of small fiber neuropathy is poorly understood, but this is the type of neuropathy that is prominently observed in the leading PN etiologies: diabetes, aging, and now COVID[7]. SFN can also arise as a result of a variety of other diseases such as autoimmune disorders including sarcoidosis, paraproteinemia, and paraneoplastic syndrome.

Limitations of Current Diagnostic Methods

Currently, small fiber neuropathy (SFN) is a major contributor to all types of neuropathy cases and is difficult to effectively diagnose in a clinical setting. Combinations of behavioral testing, patient questionnaires, skin biopsies, and nerve recordings from electromyography (EMG) of large fiber nerves are utilized for a diagnosis. Common problems that can be traced back to each of these testing methods is the fact that diagnosing neuropathy is often a painful, invasive, and costly process. Additionally, these approaches do not provide any quantitative, functional data on *small fiber nerves*, such as those innervating skin and subdermal tissues, and often result in numerous false negative or false positive tests. Skin biopsies, the gold standard diagnostic in SFN, are particularly fraught, and only a handful of labs in the country provide reliable analyses through immunostaining and quantification of intra-epidermal nerve fiber (IENF) density in the skin sample. The lack of specific *functional* testing for small fiber neuropathy can result in unnecessarily long and arduous periods of diagnostic testing for both patients and clinicians.

The New Detecting Early Neuropathy (DEN) Medical Device for Functional Assessment of Transdermal Small Fiber Nerve Activity

To provide a new means of functionally testing for SFN and DPN, we developed a new medical device. The Detecting Early Neuropathy (DEN) device is a needle electrode array consisting of 9 needle electrodes arranged in a 3x3 grid, with each needle connected to a copper trace on a single printed circuit board (PCB) that terminates at a cable connector. The DEN device needles are inserted into the skin, where they penetrate to various subcutaneous tissue depths in order to measure nerve electrical activity over time, or in response to various stimuli. The purpose of this study was to validate and optimize the DEN device in a mouse model of DPN, and to determine if the DEN device can record from small fiber nerves in human.

METHODS

Construction of DEN Device Prototype for Mouse

The construction of the DEN device began with a prototype for assessing optimal spacing of the array needle electrodes. Plastic spacers were incorporated to allow varying penetration depth into the skin. The printed circuit board, or PCB, consists of 9 positions/holes arranged in a 3x3 grid, with each position attached to one needle electrode and a copper trace within the PCB, connecting to a single output pin of an edge connector (Fig. 1A-E). The experimental recording setup contained 4 amplifiers, from which each amplifier recorded from two needle outputs, one

(+) and one (-) (Fig. 1F). Four different needle array designs were used, each with varying needle depths, in order to determine the optimal depth at which to record activity within the scWAT depot, as well as validate the functionality of the device during the recording process. After a preferential depth of penetration was determined, a single style of array was chosen to use for the duration of the high fat diet cohort recordings.

Animals and Dietary Intervention for Mouse DPN Model

Following validation of device nerve electrophysiology in cricket leg and limulus nerve, this study utilized weight-matched and age-matched male C57BL/6J (Jackson Laboratory, Bar Harbor, ME; stock number 000664) mice obtained from The Jackson Laboratory. Animals were housed with 4 per cage, providing for socialization in a temperature and humidity-controlled environment with a 12/12 h light/dark cycle. Access to food and water was maintained ad libitum and cages were changed daily. Following all recording sessions, animals were euthanized using CO_2 followed by cervical dislocation. To achieve a diabetic state known to induce functional neuropathy, adult male C57BL/6J mice were fed 58% high fat diet from (Research Diets Cat #12330). Body weight was recorded weekly, and adiposity was assessed at the end of the study by weighing intact subcutaneous adipose depots after surgical removal. Mice were evaluated via electrophysiological flank skin/subdermal recordings in groups (N=4) at 2 weeks, 6 weeks, 10 weeks, 16 weeks, and 25 weeks after the start of the dietary intervention. Additionally, healthy control (chow-fed mice (N=4)) were evaluated at the same time points with flank skin/subdermal nerve recordings comparing the high fat diet mice against healthy control mice.

Measurement of tissue nerve activity with DEN device- MOUSE

Mice were administered 5% isoflurane for 3-5 minutes in a takedown chamber to ensure deep anesthetization, then continuously administered 1.5 - 2.0% isoflurane through a fitted nose cone for the duration of the recording. Complete recording sessions typically lasted no longer than 45 minutes. Skin directly above the inguinal scWAT (~1x1 inches) was shaved of fur using a razor blade to allow for better needle array penetration through skin. The mice were then placed inside a faraday cage, which redistributed charges from the exterior electric field in the recording room within a copper wire mesh, in turn preventing most exterior signal noise from interfering in the raw data. The DEN device needles were inserted into the shaved portion of the skin, directly over the subiliac lymph node, a region of known high density innervation[11], then reinserted ~1mm adjacent to the original penetration site twice, for a total of three penetration locations on each mouse during each recording session (Fig. 3A). All representative traces of raw data were taken within the first minute of recording from Position 1, Time 1. Following DEN insertion, the device was

maintained in place by loosely tying the holding edge of the DEN device around the animal with plumber's tape (Fig. 3B) and a 5-minute recording of nerve electrical activity was begun using a 4 channel, BIOPAC MP160 system. All mice were killed via cervical dislocation at the conclusion of each session.

Measurement of tissue nerve activity with DEN device- HUMAN

For all human recordings, the DEN device was inserted into the lateral human calf. Prior to insertion, the skin was disinfected with _70% ethanol and left to air dry. The subject's leg was placed inside a Faraday cage and a ground was connected from the Faraday cage to the subject via an EKG surface skin electrode placed approximately 6 inches rostral of the DEN device. The DEN device was also disinfected with 70% ethanol and left to completely dry before insertion. Following DEN needle electrode insertion, the device was maintained in place using self-adhesive athletic tape wrapped around the calf and DEN (Fig. 5C). Recording of nerve electrical activity was begun using the BIOPAC MP160 system. The BIOPAC recording system consisted of 4 individual amplifiers, each having two inputs. All 4 differential amplifier inputs were connected (each with a + and - input) to a 10-pin flat ribbon cable which was connected to the array via the PCB edge connector. The 9th input into the cable could be used as the ground reference, and the 10th input (located centrally on the array) was left open (to be used as a stimulation electrode if desired). For all recordings (unless noted otherwise), amplifier settings were adjusted to 1000x gain, 0.5Hz high pass filter (HPF) and 3kHz low pass filter (LPF). The raw data from this experiment was analyzed manually using the BIOPAC AcqKnowlege software. All recordings were taken at 40kHz, allowing for the potential visualization of single action potentials. Due to the location of DEN insertion in the human calf, EKG signal was not factored into the rate and duration of patterned neural signaling observed with the BIOPAC software.

Recording with EKG

When recording using DEN in conjunction with EKG equipment, a secondary area of fur was shaved over the chest of the mouse in addition to the typical area of the flank. A primary adhesive electrode was placed over the shaved area of the chest of the mouse. A secondary adhesive electrode was also applied to the hind paw. Both electrodes were connected to a single BIOPAC amplifier, allowing three channels to receive neural activity input from DEN and one channel to receive EKG. The DEN array was inserted into the flank of the animal as described in normal recording process, and both activity types were compared.

Skin intra-epidermal nerve fiber (IENF) density quantification

Glabrous hind paw skin and hairy flank skin (above the inguinal scWAT depot) was excised and fixed in 2% Zamboni's fixative (Newcomer Supply # 1459A) for 2hrs at room temperature, transferred to 30% sucrose in 1XPBS overnight (until tissues sink), and embedded in OCT (Tissue-Tek cat #4583 Miles, Inc.) with orientation noted. Tissues were sectioned at 25 µm onto glass slides. Tissues were placed in 0.03% Typogen Black for 20 min at room temperature to quench autofluorescence, then rinsed in 1XPBS 3x 5min or until rinse ran clear. Tissue sections were blocked in 200 uL blocking solution (1X PBS/0.3% Triton X-100/5% BSA) at room temperature for 1 hr and then incubated in primary antibody (Proteintech rabbit anti-PGP9.5 (14730-1-ap), 1:1000) for 1 hr at room temperature and then moved to 4ºC for incubation overnight. Sections were rinsed 3 x 1hr in 1XPBS and incubated with secondary antibody (AlexaFluor Plus 594 highly cross absorbed, 1:1000 (Molecular Probes)) for 1 hr at room temperature and then moved to 4ºC for incubation overnight. Sections were rinsed 3x1hr with 1XPBS and then incubated in 100 ng/mL DAPI solution for 15 min. A final 3 x 10 minutes in distilled H_2O rinse is performed and slides were then mounted with a drop of mounting fluid (Prolong Gold, Thermofisher #P36931) and a No. 1.5 glass coverslip for imaging on a Leica Stellaris 5 confocal microscope. Quantification of imaging was performed on Fiji Image J. The pixel/µm ratio was set for all measurements as 4.5539 pixels/µm. The boundaries of the region of interest (ROI) was created by outlining the entire epidermal layer on the 40x image. A measurement of the total ROI area was taken. The PGP9.5 channel was isolated and a consistent histogram criterion for thresholding was selected as 'internodes' across all images. The area of the thresholded nerves expressing PGP9.5 was measured and the relative nerve fiber density was calculated: thresholded nerve area / total ROI area.

BIOPAC Manual Data Analysis

The BIOPAC recording system consisted of 4 single amplifiers each containing two inputs. For the DEN needle array, all 4 differential amplifier inputs were connected (each with a + and - input) to a 10-pin flat cable for direct connection to the array. The 9th and the 10th input (located centrally on the array) was left open. The stimulation recording settings were designed for recording compound action potentials. For basal recordings, the amplifier settings were adjusted to 1000x gain, 0.5Hz high pass filter (HPF) and 3kHz low pass filter (LPF). For stimulation recordings, the amplifier settings were adjusted to 200x gain, 0.5Hz HPF, and 3kHz LPF. The raw data from the measurement of tissue nerve activity with the DEN device for mouse experiments was analyzed manually using BIOPAC AcqKnowlege software. Time periods were identified in

which the first, second, and third recording locations occurred. An initial scan through the recording functioned to identify commonly occurring patterns of signals that existed in the raw data. Then, three small time (~3-8 sec) intervals within the zone recording were chosen at random to analyze in depth. If familiar patterns of activity were observed within the chosen interval, the amplifier(s) on which the signal occurred as well as the size and duration of the signal were both recorded for reference.

BIOPAC Semi-automated analysis

Data analysis was performed with BIOPAC AcqKnowledge software. The spikes subject to investigation all had local voltage maxima and minima that could be defined in a cycle using the Find Cycle Peak Detector. To do this, event markers were placed at instances where a local maximum in voltage was above, or a local minimum below, a threshold that was defined based on the background noise. Using the Find Cycle Peak Detector, cycles were identified with maxima being the start events and minima being the end events, or vice versa if minima preceded maxima. Data generated and exported to excel from the Find Cycle Peak Detector included time of start event, change in time (Δt) between start and end event, maximum voltage in the cycle (M), minimum voltage in the cycle (m), and amplitude ($A = M - m$). By manual processing in excel, spikes defined as cycles were excluded if parameters were not physiologically relevant, i.e. if $\Delta t > 3$ msec and if $20 \text{ mV} < A < 60 \text{ mV}$ was not true. After exclusion of physiologically irrelevant spikes, change in time between any given starting event and the subsequent starting event (ΔT), otherwise known as the interspike interval, was calculated. An approximation for instantaneous rate of spikes was calculated using the formula $1/\Delta T$, and instantaneous rates that were physiologically irrelevant were excluded from analysis. To make comparisons between individual mice fed chow diet (N = 4) and 2, 6, 10, 16, or 25 wk HFD (each group N=4), instantaneous rates of spikes were averaged in intervals of 10 sec up until 350 sec. Only data in the first 350 sec of recordings were used to minimize the effect of anesthesia on comparisons between animals.

Statistical Analysis

Mice were age and body weight matched and randomized to treatment groups. All plotted data represent mean +/-SEM. Statistical calculations were carried out in Excel or GraphPad Prism software (La Jolla, CA, USA), utilizing ANOVA, or Student's T-test as indications of significance (specified in Figure legends). Error bars are SEMs. For all figures, $*p < 0.05$, $**p < 0.01$, $***p < 0.001$, $****p < 0.0001$.

Randomization, Blinding, Replicates, Inclusion/Exclusion Criteria

For animals studies, mice were aged matched and randomly assigned to a dietary group. A total of 4 biological replicates were evaluated in nerve activity recordings for each dietary group. Experimenters were not blinded to animals group assignment during nerve recording sessions; but experimenters were blinded for the assessment and analysis of nerve recording data. All measured data was included in analyses and reported.

Ethical statement

All procedures and handling of animals were performed in accordance with the University of Maine's Institutional Animal Care and Use Committee (IACUC), to comply with the guidelines of the PHS Policy on Humane Care and Use of Laboratory Animals, and Guide for the Care and Use of Laboratory Animals. This study was approved by the University of Maine's IACUC, under protocol A2020-07-05.

RESULTS

There were four major goals of this project, which included: 1) validating the functionality of the DEN device through testing in invertebrates and control mice, 2) determining the optimal tissue depth, needle fabrication, and anatomical placement of the microneedle array for mouse studies, 3) comparing control recording data with a time-course of diet-induced DPN progression in mice, and 4) fabricating a human prototype for testing DEN recordings in human skin.

Device designs for mouse model and human use

The fundamental components of the DEN were present in both mouse and human device prototypes, while major differences between species designs included device size and flexibility of the array (**Fig. 1**). **Figure 1A-B** illustrates the DEN as optimized for use in our mouse models. Each array had three parts: a base, cover, and stand. The base and covers had nine cutouts, in a 3x3 array. Custom needle electrodes were inserted into the base, which were used to collect data from subjects. The second-generation mouse prototypes used in this study had needle electrode centers 3.25mm apart. Arrays were designed to have penetration depths up to 2.5mm. Arrays either had the same penetration level for all nine needle electrodes in the array or had varying depths. The base, cover, and stand were 3D printed with Formlabs Form 2 printer with the "standard" resin, which is hard and sturdy. The needle electrodes were housed in a base needle electrode holder, where the needle electrodes extend out the bottom of the holder. When

the holder was placed onto a subject, the needle electrodes penetrated through the skin to make the transdermal recordings. A printed circuit board (PCB) connected to a ribbon cable was used to electrically connect the needle electrodes to a recording and amplification system. Following validation in the mouse models, a first generation human prototype was constructed and tested in two healthy volunteers. The PCB for the mouse prototypes (**Fig. 1A-B**) is a glass reinforced epoxy (green), and a polyimide laminate in the human prototypes (**Fig. 1D-E**). The major differences between the mouse and human prototypes were the spacing between the needle electrodes, penetration depth of the needle electrodes into the intended subjects, and the rigidity of the prototypes.

The DEN prototypes designed for human use contained the same components as for mouse, i.e. PCB, needle electrodes, 3D printed needle base, cover, stand and cable with connector. A diagram to visualize the assembly of the components into the prototype is shown in **Fig. 1C, left panel**). Needle electrodes are inserted into the needle electrode base (**Fig**. **1C, middle panel**), which is designed to allow 4mm of the needles to extend out of the base. The human needle electrode base was designed to maximize flexibility in the array while maintaining sufficient support for each individual needle electrode, so that the array could conform to the human skin surface while keeping each needle in proper alignment for orthogonal penetration. The final design involved a 3x3 array of rigid individual needle holders connected by flexible arms, and mechanical attachments to connect the needle electrode holder to the flexible PCB. The final design of the individual needle holders were 7 mm x 7 mm x 4.75 mm rectangular blocks with 2.3 mm x 2.3 mm openings at the center, into which the custom needle electrodes were pressed and held firmly in place. The connectors between the individual needle holders varied in size depending on the overall size (and spacing) of the needle array. Three different prototype sizes were developed for the project, two of which are shown in **Fig**. **1E**. The smallest had the distance between needle centers 10.16mm apart. The middle prototype had needle centers 12.7mm apart, and the largest had centers 19.05mm apart. The sizes reflected a wide range to test for optimal spacing for assessing neural health. **Fig. 1C** (middle panel) shows the final needle electrode holder design.

A 2mm spacer was made to be optionally added below the needle electrode base, to reduce needle penetration depth (**Fig**. **1C, right panel**). A cover for the array was created for application safety and to assist with insertion of the prototype. Because the needle electrodes extend above as well as below the needle electrode base, a cover with height greater than 5 mm is needed in order to ensure an administrator will not be at risk for a needlestick injury and to apply an evenly distributed force to all of the needles in the array of needles during insertion into

a patient's skin. Stands were designed to support an assembled prototype. The array is lifted 10 mm, to ensure needle electrodes do not come into contact with the surface. The base, spacer, cover, and stand were 3D printed with Formlabs Form 2 printer with the "Flexible V2" resin. The flexible PCB is much thinner than traditional PCBs and is specially designed to withstand bending. The flexible PCB is placed on top of the needle electrode base, and is electrically connected to the needles (**Fig**. **1D**). For both mouse and human recordings the DEN was connected via ribbon cable to signal processing hardware and the BIOPAC amplifiers (settings described in Methods section), a schematic of which is shown in **Fig. 1F**.

Validation of the DEN Device

Prior to vertebrate studies, experiments were performed in invertebrates to optimize device parameters and to confirm that nerve electrical activity was being detected and recorded. For conformation, we compared our DEN needle electrodes with commercial Natus (Natus Medical Incorporated) electrodes in cricket leg recordings. Natus electrodes are disposable electrodes often used in nerve conduction velocity (NCV) diagnostic tests in mouse and human[15]. Similar to the custom DEN needle electrode, the Natus electrode is made of stainless steel. In the experiment a single leg was removed from two anesthetized crickets. In each leg, an electrode, either DEN or Natus, was placed in the coxa, and a ground was placed into the tarsus. Following electrode insertion, recording was started. A mechanical stimulation was supplied to the cricket leg through a puff of air. This stimulation caused compound action potentials in the leg to occur, which were recorded and displayed using the BIOPAC Acqknowledge software (**Suppl. Fig. S1A**). Limulus nerve was used to determine optimal needle spacing for differential recordings within the DEN array (**Suppl. Fig. S1B**).

Three experimental trials were performed in anesthetized mice for the purpose of validating the DEN electrodes against commercial Natus electrodes, as well as to test the functionality of the DEN second generation mouse device as a unit. In all mouse validation studies, the Natus electrode provided stimulation when necessary and recordings were made using both Natus and custom DEN needle electrodes.

The first experiment used a stimulation from the BIOPAC system into the mouse's sciatic nerve and recorded the response from the right front paw. Since stimulation in this experiment was electrical, a stimulus artifact was expected to appear in the raw recordings. Stimulus artifacts appear as a sudden spike of voltage in recordings, followed by a similar spike return to voltage values prior to stimulation, and ended with a plateau at the initial voltage amplitude prior to a stimulus response. Compound action potentials (CAPs) follow the stimulus artifact and typically

appeared as signals with near-symmetry above and below the x-axis, with a smooth curve at the peak. CAPs were detected at a 50mV stimulation and 200x gain from all three recording differentials (**Suppl. Fig. S1C top 3 panels**).

The second experiment recorded from mouse flank without stimulation and confirmed that the DEN electrodes could obtain nerve recordings from a live mouse, as shown by response to (**Suppl. Fig. S1C bottom panel**). The electrodes recorded differentially from two custom needle electrodes placed in the tail, with a ground in the front right paw of the mouse. Recording without stimulation also ensured that all connections, hardware, and software functioned properly. The large 0.5mm, 1.0mm, and 1.5mm penetrating array designs were used.

The third experiment recorded from the mouse flank using the complete DEN device, plus one custom needle electrode penetrating into the paw, similar to the NCV diagnostic test done in humans. All differentials displayed a stimulus artifact at a 200x gain when a 50mV stimulation was supplied to the array (**Suppl. Fig. S1D**). It was shown that the differentials located closest to the stimulation show the greatest stimulus artifact. In addition to varying stimulus artifact responses, CAPs can be seen clearly in Channels 2 and 4 of the four differentials.

To determine if enhanced conductivity was necessary for recordings obtained from stainless steel needles, a thin silver wire was placed inside the coated needle electrodes used for recording, the wire was then removed while the DEN device recorded from Position 1, Time 1 of a control mouse (see **Fig. 3A** for anatomical location). After anesthetization and insertion of the array, the silver wire was pulled from each single needle. Recording was stopped and re-started after the removal of each wire. The silver wires were removed according to the channel each needle corresponded to, with the wire removed in ascending channel order (Channels 1, 2, 3, then 4). Finally, the DEN device recorded with no silver wire for several minutes. The raw data recordings showed no difference in the prevalence or rate of electrical activity recorded from the control mouse (**Suppl. Fig. S1E**).

Neuropathy Time Course Study

In order to correlate nerve electrical signals measured by the DEN to known assessments of PN we employed a mouse model of diabetic peripheral neuropathy that is induced by 58% high fat diet feeding for at least 16 weeks, as previously validated by[16] and independently by our laboratory. We employed this high fat neuropathy-inducing diet (HFND) over a time course in order to evaluate changes in peripheral nerve activity at pre-diabetic stages, as well as early diabetic and neuropathic stages of diabetes in mice. A diagram of study design is sown in **Fig. 2A**. Assessments at multiple time points provided a continuous view of how earlier stages of

neuropathy may affect subdermal recordings in the skin. It is important to note that functional large fiber neuropathy has been seen in mice at 16 weeks after consuming a high fat diet, but in previously published studies nerve density remained consistent in the skin at this time point[16]. Therefore, the 2 week, 6 week, and 10 week mouse cohorts evaluated in this study were included to precede the point at which functional neuropathy was expected to occur. But small fiber nerve activity measurements at these points may show patterns different from lean (chow) controls. In particular, the recording of any compensatory effects prior to measurable functional neuropathy in mice served as a point of interest throughout this project. As expected body weight and scWAT weight increased the longer mice remained on HFND (**Fig. 2B**). Intra-epidermal nerve fiber (IENF) staining showed steadily decreasing density of innervation in the intra-epidermal layer as time on HFND continued, with a significant decrease in nerve density at the 16-25 weeks HFND time point compared to 2 weeks on HFND (**Fig. 2C**).

Three major anatomical zones were used for recordings in mice using the DEN device. For Position 1, Time 1, the array was centered above the subinguinal lymph node (SiLN) region since this area has been shown to have a dense innervation of nerve fibers in the inguinal scWAT[11]. Position 2, Time 2 was located approximately 1mm cranially to Position 1 Time 1, and Position 3, Time 3 was located approximately 1 mm caudal to Position 1, Time 1 (**Fig. 3A**). Moving the needle array slightly throughout the recording sessions allowed for variation in the types of activity seen, as well as increased the chance that the array would become positioned optimally near a single nerve axon, or bundle of nerve fibers. Activity could also be tracked through positions for interpretation of distance moved closer or further from a site of potential neural activity.

The DEN recorded a variety of nerve signatures including putative action potentials (PAPs) in mice across all time points in the HFND longitudinal study. Each recording zone was chosen based on proximity to the SiLN (**Fig. 3A**). Prior to recordings, mice were anesthetized and stabilized for the insertion of the DEN array (**Fig. 3B**). There were three main types of activity identified which occurred across all three recording zones in both control and HFND treated mice. The first type of activity was spike trains, defined as the repetitive and constant firing of PAPs over a set period of time (**Fig. 3C, Suppl. Fig. S2A**). This property gave spike trains rates of activity which could be traced across time points of HFND. The second type of activity recorded was bursts, or the firing of many PAPs over a short period of time, typically less than 1 second (**Fig. 3C, Suppl. Fig. S2A**). Finally, single PAPs were recorded as isolated events that appeared similar to neural action potentials in nature (**Fig. 3C, Suppl. Fig. S2A**). Criteria used to identify PAPs included the presence of relative symmetry of the signal amplitude both above and below

the x-axis, a signal duration of less than 0.5 milliseconds, and the non-synchronous presence of the signal on more than one recording channel.

Since time under anesthesia was a confounding variable that was also not present in human testing, we measured impacts from anesthesia separately (**Suppl. Fig. S3A**), and verified that environmental stimulation, such as temperature sensation could be captured by the DEN (**Suppl. Fig. S3B**).

Spike Trains are Concurrent with EKG Signals

By simultaneously recording with DEN and including traditional surface electrodes placed on the mouse for EKG recording, spike train patterns were able to be manually analyzed alongside EKG signals using BIOPAC equipment and software. Upon completion of this analysis, it became apparent that spike train signals were occurring at the same time and rate as EKG signals in the mice. Both signals occurred at the same rate and fluctuated in tandem throughout the recording session (**Fig. 4A**). Interestingly, the overall rate and prevalence of spike train activity was seen to decrease significantly at early and late time points of HFND feeding (2 week and 25 week HFND cohort groups compared to chow controls) (**Fig. 4B**). At the 25 week time point PN is present and the decrease in spike train activity may potentially be indicative of cardiac autonomic neuropathy (CAN), a known condition in obesity and diabetes that is also often underdiagnosed,[17, 18]. The changes observed at the 2 week time are also interesting as leptin resistance is present in mice by 2 week of HFD feeding[19].

Optimizations of the DEN device for human studies

Upon completion of pre-clinical studies in diet-induced models of peripheral neuropathy in mice, the DEN device was optimized and tested in two healthy human subjects. Notable differences between murine skin and human skin (illustrated in **Fig. 5A**) which needed to be considered included: fewer hair follicles in human skin, the absence of $\gamma\delta$ dendritic epidermal T-Cells in the epidermis, and presence of eccrine sweat glands. Additionally, humans lack the *Panniculus Carnosus*, a muscle layer present in mice and other mammals that is involved in skin contraction, wound healing, and skin adherence to underlying tissue [20]. The spacer layer was used with the DEN device to reduce the needle penetration depth into human skin from 4mm to 2mm (**Fig. 5B**). As the human subject testing was being done on the lower leg, only the 2mm needle length array was tested. This depth of penetration allowed for skin dermal recording without reaching the subdermal layer (**Fig. 5A**). The device was inserted into the lateral calf and secured using self-adhesive athletic tape (**Fig. 5C**). Participants were asked remain still for 30

seconds, then move their foot and ankle at various points during the recording session.

Upon insertion into the skin, it was found that the DEN device recorded electrical signals from nerves in human subjects without the interference of heart EKG signals (**Fig. 5D**) observed during mouse experiments. This is attributed to the small body size of mice and consequent proximity of the DEN device to the heart. There were six major types of neural activity that occurred in human recordings: single action potentials (**Fig. 5D, i-ii**), spike train activity (**Fig. 5D, iii**), trains of CAPs/CMAPs (**Fig. 5D, iv**), individual CAPs/CMAPs (**Fig. 5D, v-vi**) which could be distinguished from trains of CAPs/CMAPs, patterned bursts of CAPs/CMAPs (**Fig. 5D, vii**), and EMG activity following foot-ankle flexion (**Fig. 5D, ix**). All human recordings were taken at a 40kHz sampling rate, as opposed to the 2kHz sampling rate used in preclinical mouse studies, in order to better visualize individual neural events as seen in **Fig. 5D** and **Suppl. Fig. S3C**. Following foot-ankle flexion, a spike in activity across all recording channels was noted (**Fig. 5E**), which is predicted to be an EMG response.

DISCUSSION

Following the initial validation studies to evaluate the performance of the DEN device, we determined that electrical stimulation was not required to record spontaneous nerve firing and field potentials from skin and transdermal tissues of live mice. We also confirmed additional settings in the early testing that were used in the diet-induced neuropathy model: the recording site (mouse flank/inguinal skin, with hair removal), the confounding cooling of the animal due to the inhaled anesthetic over time, and the placement of the mouse in a Faraday cage to shield from room electrical noise (which was further filtered out as a reliable 60Hz room noise signal with the BioPac software). This process enabled the progression into a pre-clinical mouse model of DPN, with the goal of determining if the device was able to detect changes to nerve health and integrity across the progression of diabetic neuropathy.

Over the course of this study, we confirmed that the DEN device could successfully record neural activity from both mice and humans in the basal state. A diet-induced diabetic mouse model validated that the DEN device could detect physiological changes to nerve activity signatures, associated with a worsening state of diabetes and neuropathy (as confirmed by lower IENF across the diabetic time-course). In mice, there were three major types of nerve electrical activity seen to occur during the recording process: spike trains, bursts, and single spike events. The activity measurements from the pre-clinical mouse recordings were confirmed to be of neural origin due to the duration of the signals, amplitude, and relative symmetry above and below the y-axis. Specifically, signals of ~1 msec with a 2:1 signal to noise ratio, symmetry above and below the y-axis, and occurring on only 1 channel at any given time were identified as possible nerve signals. These events were believed to correspond with various types of neural activity generated within the subdermal tissue and muscle of the mice while under anesthesia, including from the various nerve endings innervating the tissue (sensory, motor, autonomic).

By recording using both the DEN device and an EKG electrode, we discovered that the rate of spike trains was synchronous with the rate of EKG from the mice over time, and was ruled out as a small fiber nerve signal. Regardless, the ability of the DEN device to record EKG in mice may have beneficial implications when assessing patterns of EKG over a diabetic time course, such as for the diagnosis of cardiac autonomic neuropathy (CAN). The rate of both EKG and spike trains decreased notably at 2 weeks of the mice being fed HFND, a direct correlation to the expected onset of leptin resistance[21]. Leptin has been associated with the moderation of cardiac electrical properties, via inhibition of the β-adrenergic receptor, which can cause leptin to accumulate in the myocardium and result in sustained bradycardia[22]. A similar decrease in spike

train/EKG signaling rate occurred in the recordings taken from mice in the 25-week HFND time study. This change may have indicated the presence or development of CAN, a complication associated with diabetes that is often linked to an increased risk of cardiovascular mortality rate [23]. Anesthesia may have also played a role in the depression of heart rate across each recording group over time.[24]

One notable adjustment that was made during the transition from recording in mice to recording in humans was the sampling rate at which recordings were obtained. For the mouse recordings, the sampling rate was set at 2KHz, which allowed larger neural and/or muscular events such as CAPs/CMAPs and EMGs to be visualized and evaluated. Recording at 2KHz also managed the file sizes which were saved for analysis. However, when recording in humans, the sampling rate was adjusted to 40KHz in order to better visualize single action potentials alongside larger neural and/or muscular events. Since the sample size in the human trials was much smaller than the mouse studies, having a larger file did not pose any problems for analysis at 40KHz. Custom software and cloud data storage solutions are now being developed for future human testing studies at 40KHz.

Limitations of this study included not yet having a validated algorithm devoted to detecting changes in activity seen across the diet-induced diabetic mouse model. Neuright, Inc. is currently working on developing a proprietary algorithm that can be applied both to animal and human recording data. All analyses of spike train/EKG data were conducted manually or using a semi-automated analysis. By developing an algorithm which can predict the stage of neuropathy based on patterns of electrical activity recorded from DEN, we hope to automate the analysis of these recordings, making the process more efficient and accurate for the purpose of diagnosis.

In this study we have validated the functionality of the DEN as a novel functional diagnostic for SFN/DPN through recording neural activity in the subdermal tissue of basal mice as well as a diet-induced obese/diabetic/neuropathic mouse model. The differences we observed in rates of activity across each time point of HFND support the possibility that changes in frequency and/or rate of specific types of nerve activity patterns could indicate physiological changes associated with the onset of early late-stage DPN. In addition, the DEN was optimized and validated in basal humans to demonstrate the translational potential of this novel diagnostic approach. These findings support the functionality of the DEN and maintain the possibility that the DEN should be able to provide an earlier and more sensitive diagnosis of DPN and SFN for human patients in the near future.

Acknowledgements

The authors wish to thank Drs. Christopher Gibbons, Eva Feldman, Sandra Rieger, Brett Morrison, William David Arnold, Miriam Freimer, and Ben Harrison for helpful discussions; and Sarrah Marcotte and Caleb Berry for technical assistance in data acquisition and 3D printing. We thank Sabrina DiPietro for administrative assistance. We particularly want to thank our valued colleague Dr. Jan Pelletier for key insights regarding human skin related to this device development, as well as other helpful discussions and feedback. Dr. Pelletier was a stellar clinician, researcher, colleague, and supporter of this project, and her loss is already deeply felt by this research team.

Data availability

All data can be made available upon request to the corresponding authors.

Funding

This project was funded by University of Maine MIRTA and RRF funds, an NSF STTR Phase 1 to Neuright, Inc. (ID: 2014779), Maine Technology Institute (MTI) Seed and Grant funding, Neuright Inc. R&D funding, and an NIH COBRE award from Maine's Pilot Project Funding Driven program. Julia Towne and Brooke Villinski were supported by NSF REU Site: Sensor Science and Engineering grants 1460700 and 1851998, respectively.

Authors' relationships and activities

KLT and MB are co-founders of Neuright, Inc., a University of Maine spin-out and biotechnology R&D start-up company based in Maine and Ohio, which co-funded this study. Neuright, Inc. holds a licensing agreement with UMaine to continue R&D and commercialization for this device, and will conduct future human testing studies.

Contribution Statement

KLT conceived of the study and oversaw data collection, co-designed the device, and oversaw and contributed to manuscript preparation. RLS led the biomedical engineering team, co-designed the device, and contributed to manuscript preparation. MB led the research team, co-designed the device, and wrote the manuscript. LC collected data and wrote the manuscript. BV, JP, JMT, NS, ER, collected or analyzed data, or contributed to device fabrication and testing. BV also contributed to writing the manuscript. NE oversaw and consulted on the electronics, and LK oversaw and conducted the electrophysiological measurements and analyzed/interpreted data.

Figure Legends

Figure 1. DEN Prototypes. Second generation mouse prototype: (A) side view, and (B) top view. First generation human prototypes: (C) Left: Array Design. Blue component is the needle electrode holder, yellow component is the flexible PCB, and tan component is the 2mm spacer. Middle: CAD design of needle electrode holder, for 1" array. Right: 3D Printed components of Prototype. Assembled human prototype (D) side view, and (E) top view. (F) Schematic of microneedle array with header pins attached to signal processing hardware and BIOPAC hookups.

Figure 2. Study design and assessment of neuropathy. (A) Visual schematic of study design: adult (18/34 weeks), male, C57BL/6J mice were placed on a 58% high fat neuropathy-inducing diet (HFND) for various lengths of time. Critical physiological changes induced by HFND are denoted with respect to duration of HFND feeding. Assessments were performed at 2, 6, 10, 16, and 25 weeks after dietary intervention. *Neuropathy is evident by 16 weeks of HFND feeding. (B) Body weight of HFND and chow diet controls at time of assessment. Body and tissue weight data were analyzed with a one-way ANOVA and Tukey's post hoc test. For B, N = 4 per group. Error bars are SEMs. (C) IENF of glabrous hind paw skin showing PGP9.5 expression in the epidermal layer.

Figure 3. DEN placement and representative recordings from animals on HFND. (A) Visual schematic showing array insertion locations relative to the subinguinal lymph node. (B) Representative mouse from preclinical trials shown with array inserted over the left inguinal scWAT depot. (C) Representative electrophysiological traces from individual mice (mus1- mus4 per dietary group) used in the study. All representative traces were taken within the first minute after placement of array in Zone 1; each trace recording represents a 4 second duration. Voltage range remained between 0.10-0.14 mV with amplitudes of signals often appearing at greater than 2:1 signal to noise ratio. Green bar denotes spike train, yellow arrow points to a burst, red arrow points to single spike.

Figure 4. Comparison of DEN recordings to EKG signal. (A) EKG recordings using traditional skin surface electrodes (top channel) occurred in synchrony with spike train signals (bottom channel) recorded from DEN positioned in murine flank. EKG skin electrode was placed over the shaved chest of the mouse and ground was attached at the front paw. (B) Semiautomated

waveform analysis of “spike trains” for DPN time course. Two-way Ordinary ANOVA, for statistically significant findings Source of Variation is Diet. For all error bars are SEMs.

Figure 5. Optimization of DEN for human recordings. (A) Comparison of skin layers between mouse (left) and human (right) showing differences in underlying scWAT and nerve innervation. Mouse skin layers and human skin layers detailing epidermis, dermis, and scWAT. (B) Human DEN prototype with 3x3 needle array and corresponding output connections to recording amplifier channels. (C) DEN inserted into lateral human calf. (D) Single Action Potentials (i-ii) and a short burst of three APs (iii) are recorded from a human subject. The APs are each about 30 mV in amplitude within a baseline noise of about 10 mV. Durations of traces are approximately 5, 4, and 11 msec long. A train of CAPs/CMAPs (iv) recorded from subject NE. 4 pattern bursts, two early on and two later, of CAPs/CMAPs occur within a train of regularly firing CAPs/CMAPs. Peak to trough amplitudes within this eight sec trace are approximately 180 mV. Two of the CAPs/CMAPs (v-vi) from near the middle of the train show time resolved (trace durations of about 8 msec each) details of these CAPs/CMAPs, along with slower waves of electrical activity before (vi) and after (v) the CAPs/CMAPs, recorded at 40kHz. Patterned bursts of CAPs/CMAPs (vii) recorded from subject NE. The largest of the five bursts in this 1 sec trace have amplitudes of about 0.5 mV. The middle burst in (vii) is detailed in (viii). This 150 msec trace shows that a single burst is a complex of individual CAPs/CMAPs. An EMG (ix) from subject NE during ankle-foot flex one-third through this 2.5 sec trace. Maximum amplitude is about 0.2 mV. (E) Raw human subject recordings highlighting a spike in electrical activity following foot-ankle flexion (black line).

Supplemental Figure S1. Preliminary validation studies of the DEN device. (A) Validation of the DEN array vs. Natus electrode in cricket leg, recorded over 4 seconds. Black line denotes onset of mechanical stimulation. (B) Validation of the DEN array vs. Natus electrode vs. whole DEN array in healthy mice. Black line denotes onset of stimulation prior to CAP. (C) Compound action potentials in healthy mice. Black line indicates onset of mechanical stimulation prior to CAP (top 3 panels). Action potential captured by DEN array inserted into flank of healthy mouse. (D) Compound action potentials captured by the DEN in a healthy mouse following stimulation. (E) Removal of the silver wire inside the needle electrodes showed no significant difference in the recording sensitivity of DEN, as shown by the continuation of a spike train after wire removal (black line).

Supplemental Figure S2: Features of electrophysiological recordings obtained by the DEN in mice. (A) The 3 major types of activity recorded from mice: spike train activity (duration of 2msec shown), burst activity (duration of 1msec shown), and single spike (duration of 1msec shown). Baseline noise for traces were approximately 20mV. (B) Anatomy of a possible action potential (PAP) consisting of a single spike.

Supplemental Figure S3. Physiological validation of recordings and sample rate (A) Rate of spike activity occurrence over time recorded from a high fat diet animal. Black lines denote the repositioning of DEN. (B) Hot water bottle experiment with graph showing rate of spike train activity over time, with each point denoting an instantaneous rate of activity. Black line indicates start of recording after heating the mouse with a hot water bottle for approximately 5 minutes. (C) 2kHz vs 40kHz mouse recording showing difference in recording sensitivity. Both recordings taken from a HFND animal.

References

1. Bodman MA, Varacallo M. Peripheral diabetic neuropathy. *Statpearls*. Treasure Island (FL); 2022.
2. Carmichael J, Fadavi H, Ishibashi F, Shore AC, Tavakoli M. Advances in screening, early diagnosis and accurate staging of diabetic neuropathy. *Front Endocrinol (Lausanne)*. 2021;12:671257
3. Liu J, Ren ZH, Qiang H, Wu J, Shen M, Zhang L, et al. Trends in the incidence of diabetes mellitus: Results from the global burden of disease study 2017 and implications for diabetes mellitus prevention. *BMC Public Health*. 2020;20:1415
4. Andrei Cristian B, Amorin Remus P. Diabetic neuropathy prevalence and its associated risk factors in two representative groups of type 1 and type 2 diabetes mellitus patients from bihor county. *Maedica (Bucur)*. 2018;13:229-234
5. Kirthi V, Perumbalath A, Brown E, Nevitt S, Petropoulos IN, Burgess J, et al. Prevalence of peripheral neuropathy in pre-diabetes: A systematic review. *BMJ Open Diabetes Res Care*. 2021;9
6. Juster-Switlyk K, Smith AG. Updates in diabetic peripheral neuropathy. *F1000Res*. 2016;5
7. Cordova-Martinez A, Caballero-Garcia A, Perez-Valdecantos D, Roche E, Noriega-Gonzalez DC. Peripheral neuropathies derived from covid-19: New perspectives for treatment. *Biomedicines*. 2022;10
8. Yagihashi S, Mizukami H, Sugimoto K. Mechanism of diabetic neuropathy: Where are we now and where to go? *J Diabetes Investig*. 2011;2:18-32
9. Lehmann HC, Burke D, Kuwabara S. Chronic inflammatory demyelinating polyneuropathy: Update on diagnosis, immunopathogenesis and treatment. *J Neurol Neurosurg Psychiatry*. 2019;90:981-987
10. Yasuda H, Terada M, Maeda K, Kogawa S, Sanada M, Haneda M, et al. Diabetic neuropathy and nerve regeneration. *Prog Neurobiol*. 2003;69:229-285
11. Blaszkiewicz M, Willows JW, Dubois AL, Waible S, DiBello K, Lyons LL, et al. Neuropathy and neural plasticity in the subcutaneous white adipose depot. *PLoS One*. 2019;14:e0221766
12. Blaszkiewicz M, Wood E, Koizar S, Willows J, Anderson R, Tseng YH, et al. The involvement of neuroimmune cells in adipose innervation. *Mol Med*. 2020;26:126
13. Blaszkiewicz M, Gunsch G, Willows JW, Gardner ML, Sepeda JA, Sas AR, et al. Adipose tissue myeloid-lineage neuroimmune cells express genes important for neural plasticity and regulate adipose innervation. *Frontiers in Endocrinology*. 2022;13
14. Hovaguimian A, Gibbons CH. Diagnosis and treatment of pain in small-fiber neuropathy. *Curr Pain Headache Rep*. 2011;15:193-200
15. Chugh D, Iyer CC, Wang X, Bobbili P, Rich MM, Arnold WD. Neuromuscular junction transmission failure is a late phenotype in aging mice. *Neurobiol Aging*. 2020;86:182-190
16. Obrosova IG, Ilnytska O, Lyzogubov VV, Pavlov IA, Mashtalir N, Nadler JL, et al. High-fat diet induced neuropathy of pre-diabetes and obesity: Effects of "healthy" diet and aldose reductase inhibition. *Diabetes*. 2007;56:2598-2608
17. Williams SM, Eleftheriadou A, Alam U, Cuthbertson DJ, Wilding JPH. Cardiac autonomic neuropathy in obesity, the metabolic syndrome and prediabetes: A narrative review. *Diabetes Ther*. 2019;10:1995-2021

18. Agashe S, Petak S. Cardiac autonomic neuropathy in diabetes mellitus. *Methodist Debakey Cardiovasc J*. 2018;14:251-256
19. Wang CY, Liao JK. A mouse model of diet-induced obesity and insulin resistance. *Methods Mol Biol*. 2012;821:421-433
20. Zomer HD, Trentin AG. Skin wound healing in humans and mice: Challenges in translational research. *J Dermatol Sci*. 2018;90:3-12
21. Meek TH, Morton GJ. Leptin, diabetes, and the brain. *Indian J Endocrinol Metab*. 2012;16:S534-542
22. Lin YC, Huang J, Hileman S, Martin KH, Hull R, Davis M, et al. Leptin decreases heart rate associated with increased ventricular repolarization via its receptor. *Am J Physiol Heart Circ Physiol*. 2015;309:H1731-1739
23. Serhiyenko VA, Serhiyenko AA. Cardiac autonomic neuropathy: Risk factors, diagnosis and treatment. *World J Diabetes*. 2018;9:1-24
24. Constantinides C, Mean R, Janssen BJ. Effects of isoflurane anesthesia on the cardiovascular function of the c57bl/6 mouse. *ILAR J*. 2011;52:e21-31

Figure 1

A. **Side view of mouse DEN prototype**

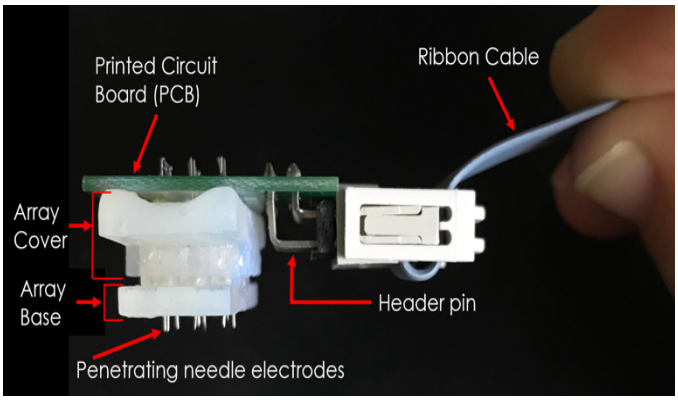

B. **Top view of mouse DEN prototype**

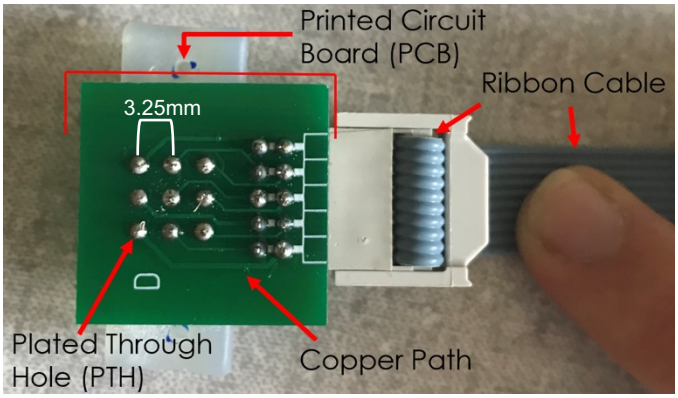

C. **Design of first-generation human DEN prototype**

Array Design

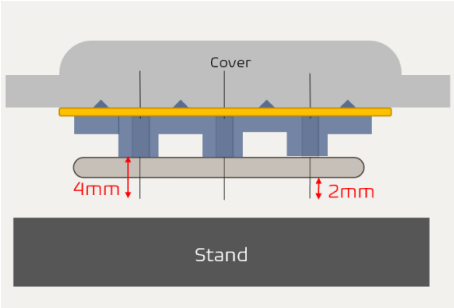

Needle Electrode Holder

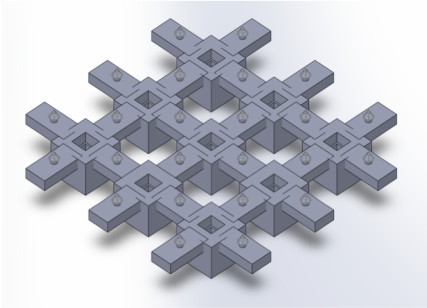

3D Printed Components

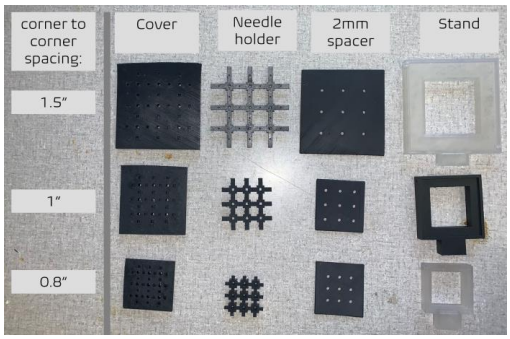

D. **Side view of first-generation human DEN prototype**

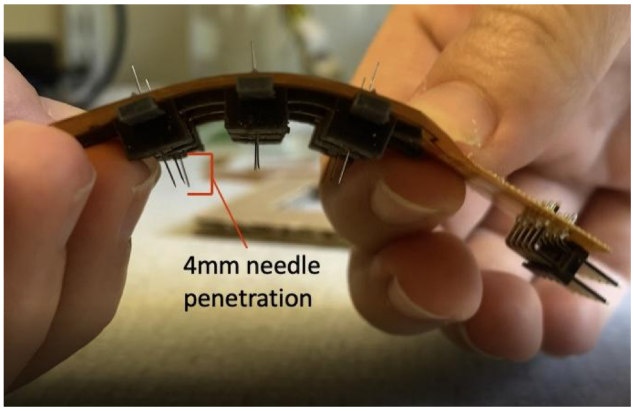

E. **Top view of first-generation human DEN prototype**

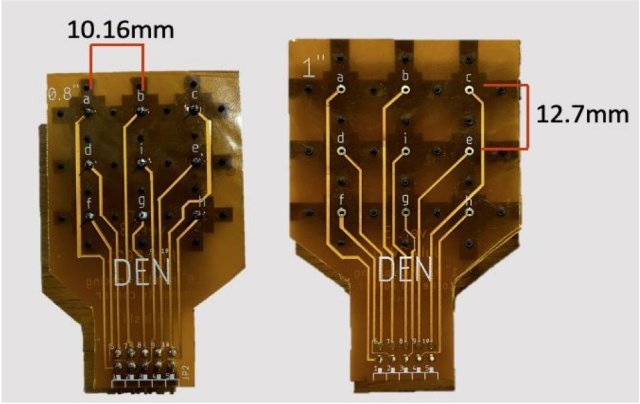

F.

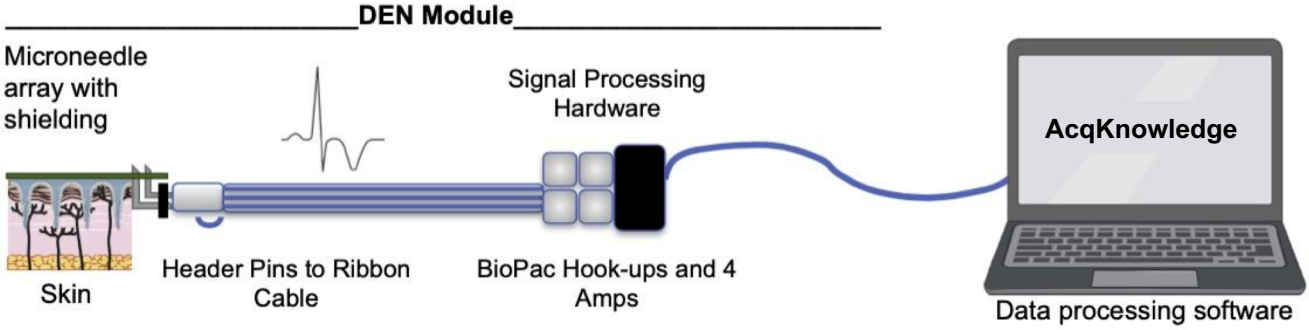

Figure 2

A.

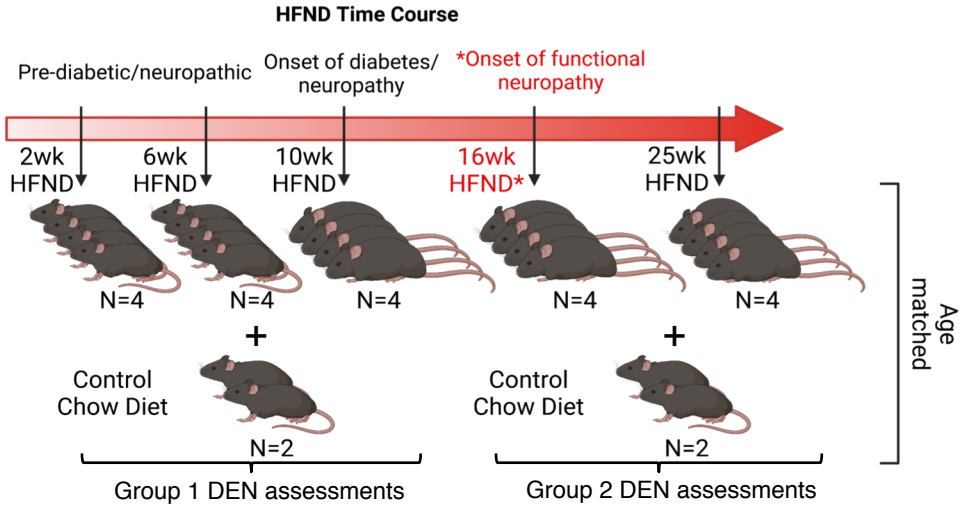
HFND Time Course
Pre-diabetic/neuropathic
Onset of diabetes/ neuropathy
*Onset of functional neuropathy
2wk HFND
6wk HFND
10wk HFND
16wk HFND*
25wk HFND
N=4
N=4
N=4
N=4
N=4
+
+
Control Chow Diet
Control Chow Diet
N=2
N=2
Age matched
Group 1 DEN assessments
Group 2 DEN assessments

B.

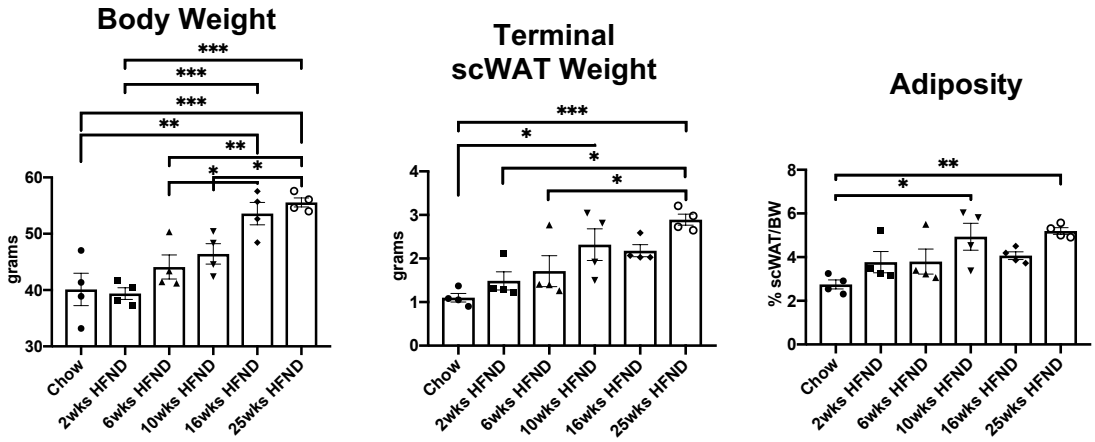
Body Weight
grams
Terminal scWAT Weight
grams
Adiposity
% scWAT/BW
Chow
2wks HFND
6wks HFND
10wks HFND
16wks HFND
25wks HFND

C.

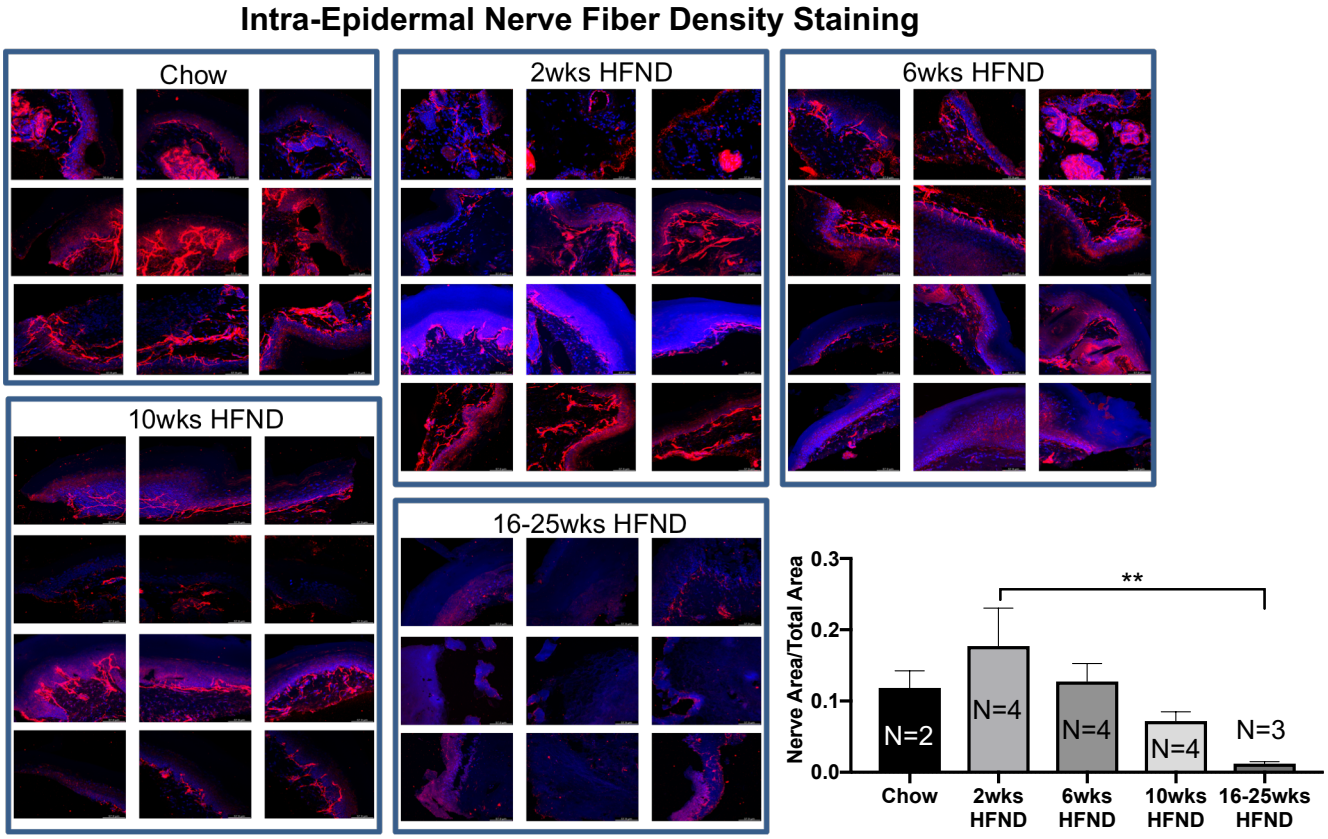
Intra-Epidermal Nerve Fiber Density Staining
Chow
2wks HFND
6wks HFND
10wks HFND
16-25wks HFND
Nerve Area/Total Area
N=2
N=4
N=4
N=4
N=3
Chow
2wks HFND
6wks HFND
10wks HFND
16-25wks HFND

Figure 3

A. **Anatomical zones of recording centered around inguinal scWAT**

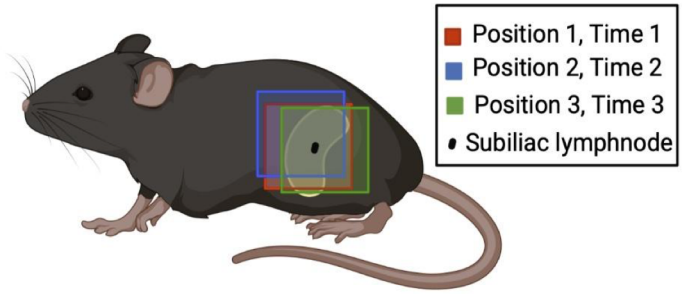

B. **DEN device recording setup**

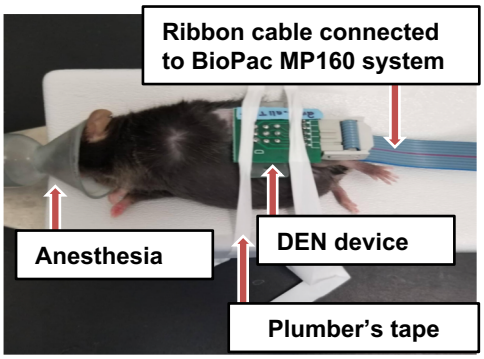

C. **Representative recordings from each animal per timepoint in the DPN study**

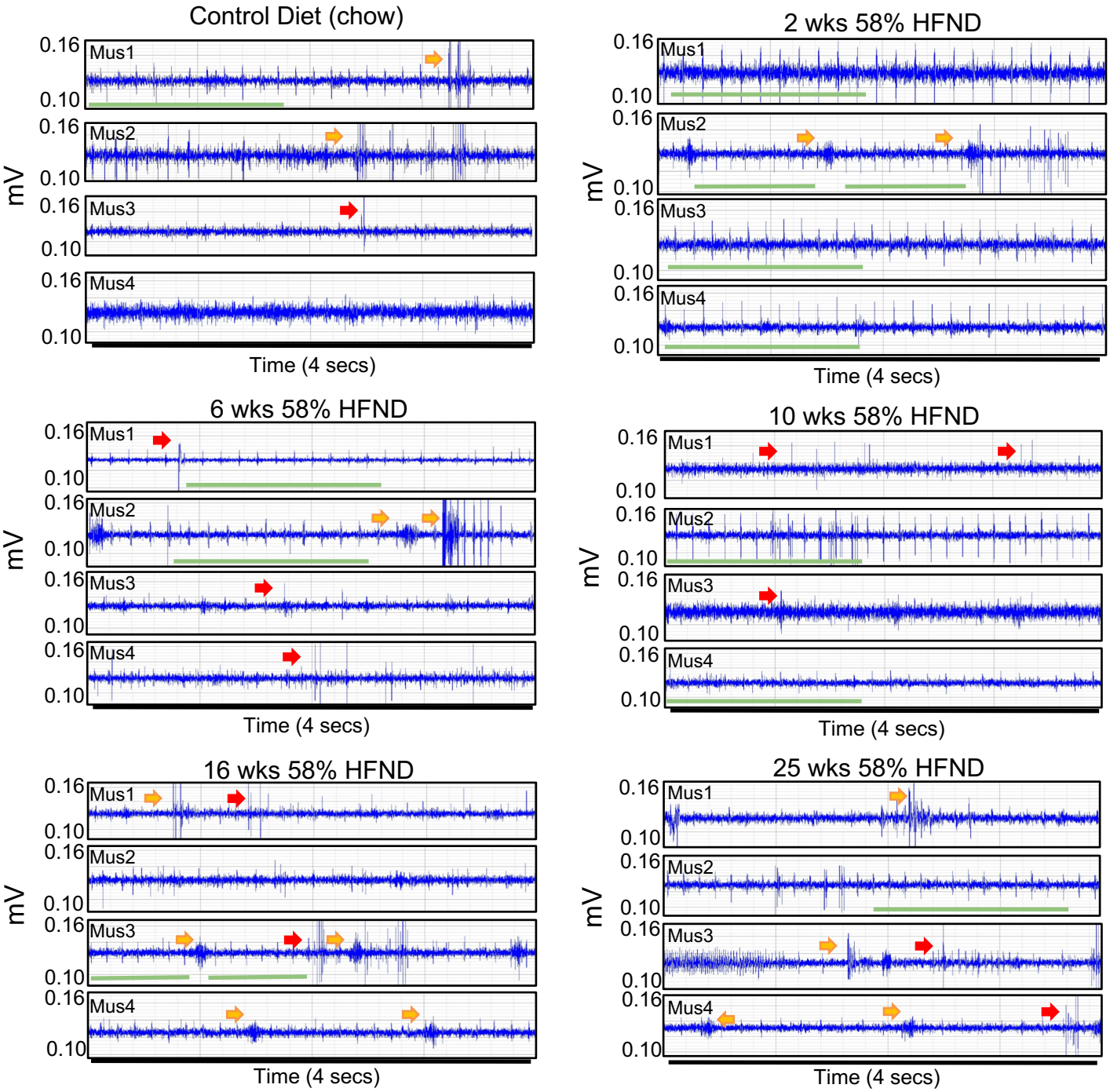

Figure 4

A. **Electrophysiological recordings from DEN vs EKG electrodes indicate spike trains are EKG but other features are not.**

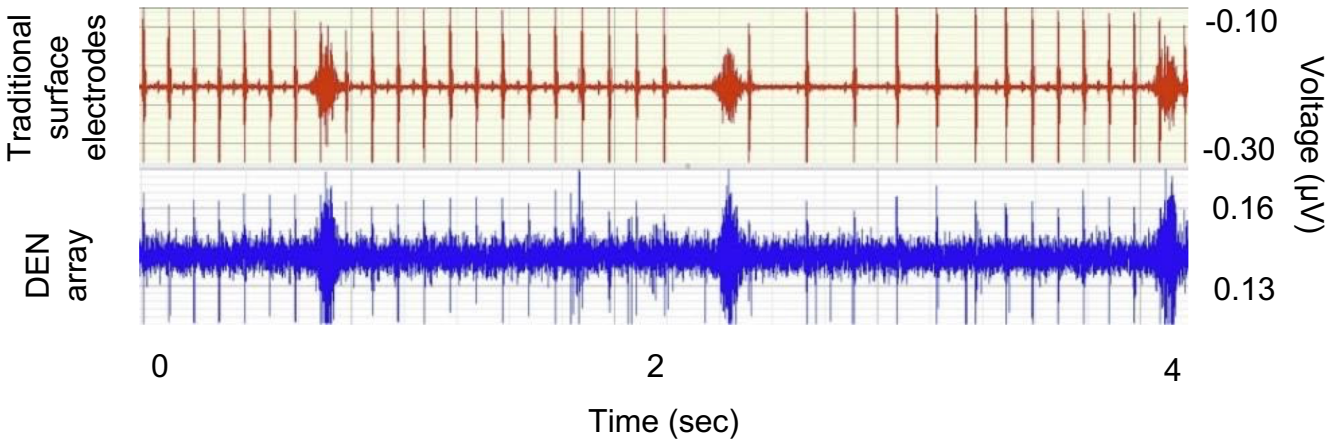

B. **Semiautomated waveform analysis of "spike trains" for DPN time course indicate periods of potential cardiac autonomic neuropathy**

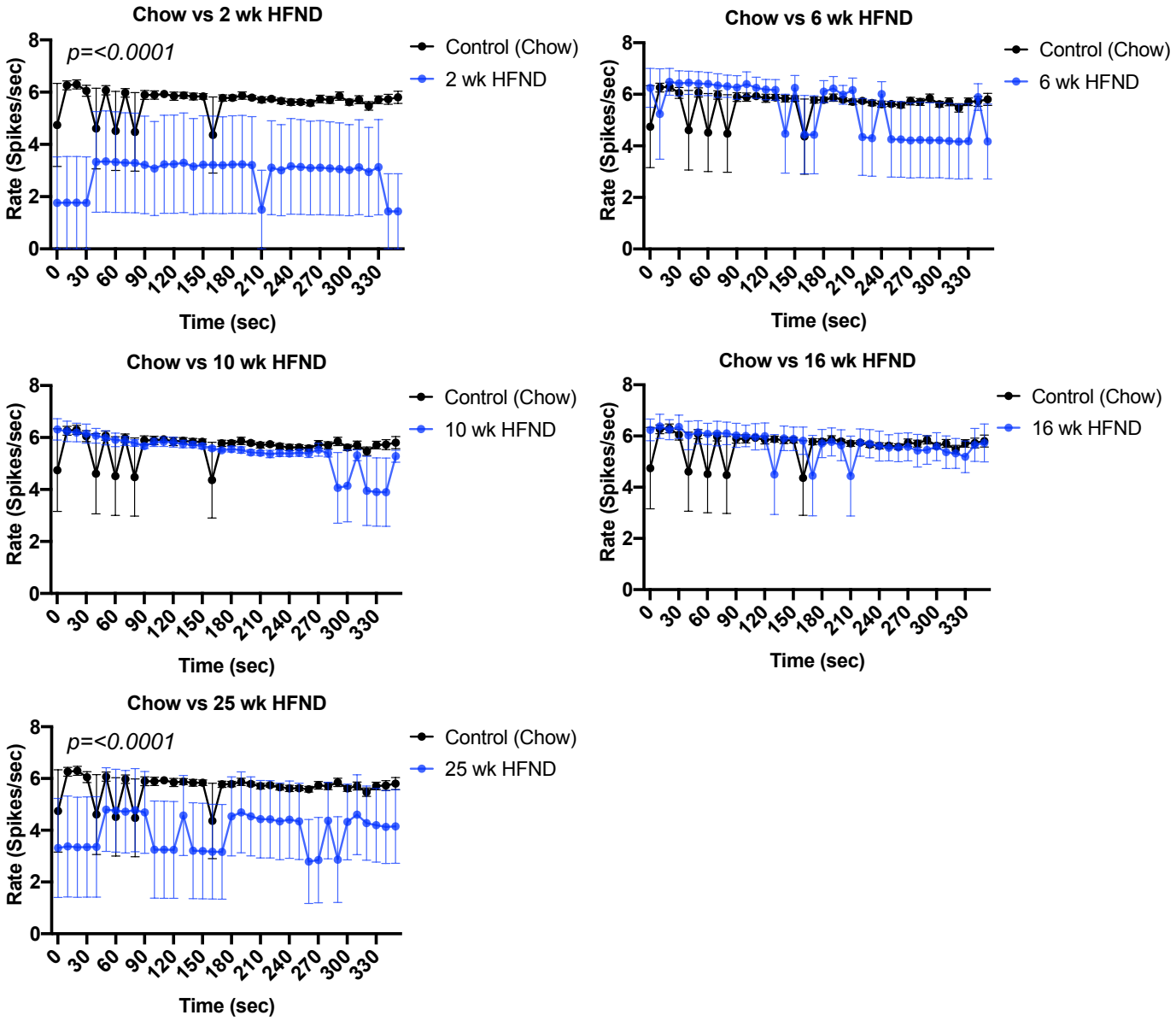

Figure 5

A. **Differences between mouse and human skin**

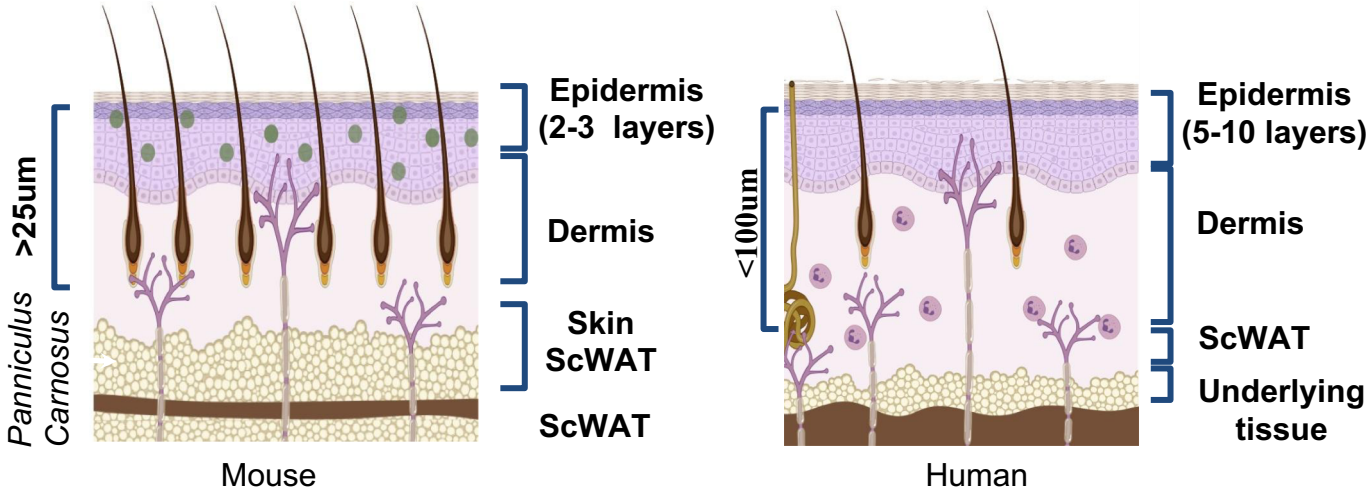

B. **3x3 needle array used in human skin**

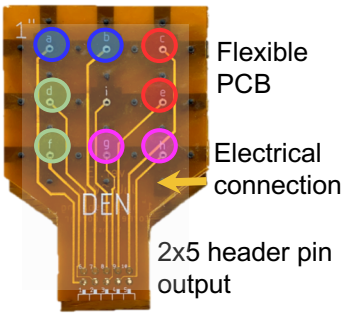

C. **Array placement in human subject's above ankle**

D. **Human DEN nerve recording features**

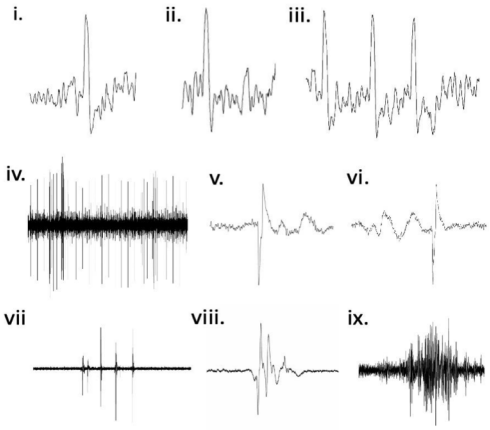
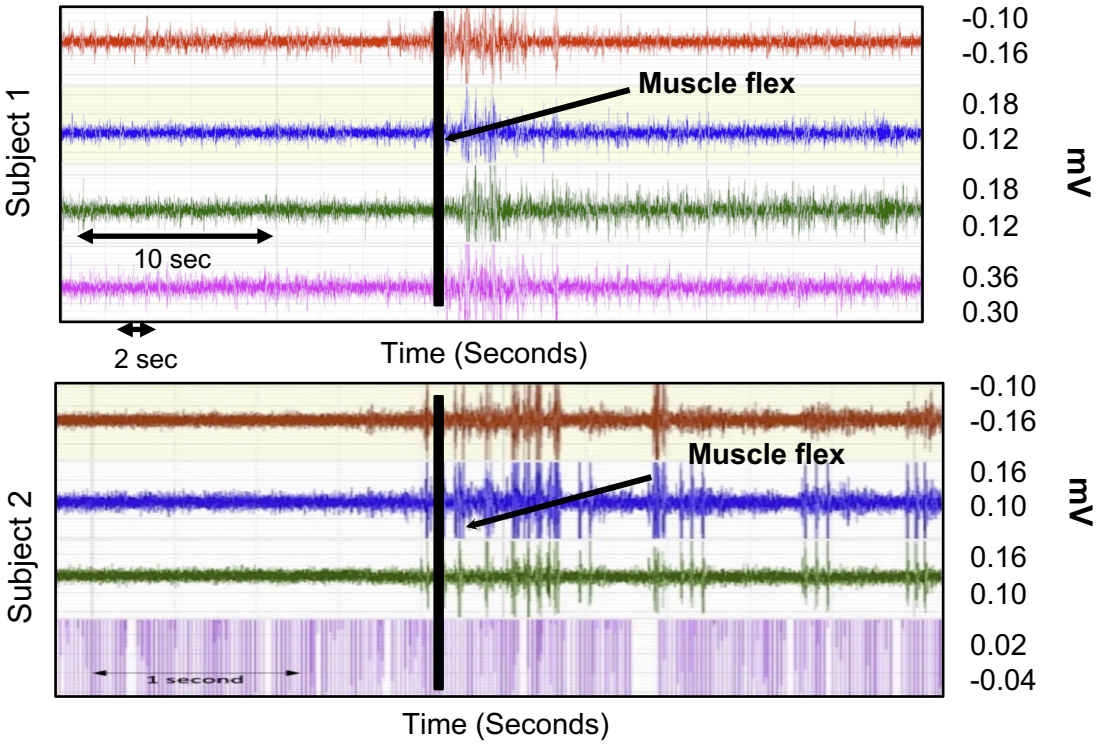
E. **Proof of concept human subject recordings**